

# UC Irvine

## UC Irvine Previously Published Works

### Title

T1rho mapping of entire femoral cartilage using depth- and angle-dependent analysis

### Permalink

<https://escholarship.org/uc/item/7mx8b8wv>

### Journal

European Radiology, 26(6)

### ISSN

0938-7994

### Authors

Nozaki, Taiki  
Kaneko, Yasuhito  
Yu, Hon J  
[et al.](#)

### Publication Date

2016-06-01

### DOI

10.1007/s00330-015-3988-5

### Copyright Information

This work is made available under the terms of a Creative Commons Attribution License, available at <https://creativecommons.org/licenses/by/4.0/>

Peer reviewed

# T1rho mapping of entire femoral cartilage using depth- and angle-dependent analysis

Taiki Nozaki<sup>1</sup> · Yasuhito Kaneko<sup>1</sup> · Hon J. Yu<sup>1</sup> · Kayleigh Kaneshiro<sup>2</sup> ·  
Ran Schwarzkopf<sup>3</sup> · Takeshi Hara<sup>4</sup> · Hiroshi Yoshioka<sup>1</sup>

Received: 19 February 2015 / Revised: 22 August 2015 / Accepted: 31 August 2015 / Published online: 22 September 2015  
© The Author(s) 2015. This article is published with open access at Springerlink.com

## Abstract

**Objectives** To create and evaluate normalized T1rho profiles of the entire femoral cartilage in healthy subjects with three-dimensional (3D) angle- and depth-dependent analysis.

**Methods** T1rho images of the knee from 20 healthy volunteers were acquired on a 3.0-T unit. Cartilage segmentation of the entire femur was performed slice-by-slice by a board-certified radiologist. The T1rho depth/angle-dependent profile was investigated by partitioning cartilage into superficial and deep layers, and angular segmentation in increments of 4° over the length of segmented cartilage. Average T1rho values were calculated with normalized T1rho profiles. Surface maps and 3D graphs were created.

**Results** T1rho profiles have regional and depth variations, with no significant magic angle effect. Average T1rho values in the superficial layer of the femoral cartilage were higher than those in the deep layer in most locations ( $p < 0.05$ ). T1rho values in the deep layer of the weight-bearing portions of the medial and lateral condyles were lower than those of the corresponding non-weight-bearing portions ( $p < 0.05$ ). Surface

maps and 3D graphs demonstrated that cartilage T1rho values were not homogeneous over the entire femur.

**Conclusions** Normalized T1rho profiles from the entire femoral cartilage will be useful for diagnosing local or early T1rho abnormalities and osteoarthritis in clinical applications.

## Key Points

- T1rho profiles are not homogeneous over the entire femur.
- There is angle- and depth-dependent variation in T1rho profiles.
- There is no influence of magic angle effect on T1rho profiles.
- Maps/graphs might be useful if several difficulties are solved.

**Keywords** T1rho · Entire femoral cartilage · Angle and depth analysis · 3D graph · Surface map

## Abbreviations and acronyms

3D	Three-dimensional
OA	Osteoarthritis
MC	Medial femoral condyle
LC	Lateral femoral condyle
T	Femoral trochlea

✉ Hiroshi Yoshioka  
hiroshi@uci.edu

<sup>1</sup> Department of Radiological Sciences, University of California Irvine, 101 The City Drive South, Rt. 140, Bldg. 56, Orange, CA 92868, USA

<sup>2</sup> School of Medicine, University of California Irvine, Irvine, CA, USA

<sup>3</sup> Department of Orthopedic Surgery, University of California Irvine, Irvine, CA, USA

<sup>4</sup> Department of Intelligent Image Information, Division of Regeneration and Advanced Medical Sciences, Gifu University Graduate School of Medicine, Gifu, Japan

## Introduction

Osteoarthritis (OA) is the most common type of arthritis and a leading cause of pain. In 2010 in the United States, it represented the 11th most common cause of disability, and was responsible for 2.7 % of all years lived with disability [1, 2]. The social cost of OA can be between 0.25 % and 0.50 % of a country's gross domestic product (GDP) [2].

New and advanced therapeutic modalities are being developed for the treatment of OA, including new chondroprotective and chondro-regenerative drugs, mesenchymal stem cell therapy,

osteocondral autograft transfer, and autologous chondrocyte implantation [3]. Therefore, it is important to detect early degenerative changes in cartilage in vivo and to understand its natural progression in order to treat OA.

New MR techniques for cartilage evaluation have recently been developed, and enable us to assess proteoglycan content, collagen content and orientation, water mobility, and regional cartilage compressibility using T2 and T1rho mapping, sodium MRI, delayed gadolinium-enhanced MRI of cartilage (dGEMRIC), and diffusion tensor imaging [4–8]. Increases in T2 relaxation time of cartilage have been associated with loss of collagen matrix anisotropy, which is a result of increased permeability of the matrix in degenerated cartilage. In contrast, T1rho imaging of cartilage shows a strong correlation between T1rho values and cartilage proteoglycan content depletion, one of the earliest degenerative cartilage changes in OA [4, 9, 10]. T1rho mapping has been a more sensitive indicator for cartilage degeneration than T2 mapping, and has enabled early detection of cartilage degeneration in early OA patients before gross morphological change occurs [4, 11].

However, what can be considered a normal range of T1rho values at specific locations of the knee is not well understood. There are also no available data about variations in T1rho measurements, especially regarding the depth and angle dependence of T1rho values over the entire femoral cartilage. This is in contrast to the well-known angle dependence that exists in T2 profiles [12]. Many reports have recently been published regarding T1rho values of healthy and damaged knee cartilage, although the methodology of segmentation and analyses varies among them (Table 1) [13–32]. The number of slices utilized in knee cartilage segmentation in most reports is typically only one to several slices, and not all of the slices from the entire knee. There are also no previous publications or reference standards describing the entire femoral T1rho map profile in normal subjects, with analysis of cartilage layer variations. This paucity of data, in turn, makes the clinical diagnosis of early OA with T1rho mapping difficult to achieve. In order to successfully apply T1rho mapping in clinical use, it is important to understand the normal T1rho profiles for the entire knee cartilage.

Therefore, the purpose of this study was to create normalized T1rho profiles of the healthy entire femoral cartilage with surface maps and 3D graphs using angle- and depth-dependent analysis, and to evaluate the usefulness of this approach.

## Materials and methods

### Subjects

We recruited 23 healthy volunteers (mean age, 28.9 years; range, 19–38) for participation in this study. Inclusion criteria

for all subjects included asymptomatic individuals between 18 and 40 years of age, with no prior history of knee injury or surgery. We excluded three subjects from the study, including one subject who had a large knee which could not fit the knee coil, and two subjects with claustrophobia. The study was approved by our institutional review board, and conformed to the tenets of the Declaration of Helsinki. Written informed consent was obtained from each subject.

### MR imaging protocol

All MR studies were performed on a 3.0-T unit (Achieva, Philips Healthcare, Netherland) utilizing an 8-channel knee receive-only RF coil. Sagittal T1rho images of the knee were acquired with spoiled gradient echo (SPGR) sequences. All sagittal images were obtained without oblique angulation, parallel to the static magnetic field (B0). The acquisition parameters were as follows. SPGR: mode=3D, fat saturation method=PROSET, repetition/echo time (TR/TE)=6.4/3.4 ms, band width=475 Hz, echo train length (ETL)=64, number of excitations (NEX)=1, field of view (FOV)=140×140 mm, slice thickness/gap=3/0 mm, flip angle=10°, image matrix=512×512 mm, number of slices=31, effective in-plane spatial resolution=0.27×0.27 mm, acceleration factor=2, spin-lock frequency=575 Hz, duration of spin-lock (TSL)=20/40/60/80 ms, acquisition time=4 min 09 s×4. Parallel imaging was used on all imaging sequences utilizing sensitivity encoding (SENSE) with an acceleration factor of 2. Routine knee sequences, including fast spin-echo two-dimensional (2D) fat-suppressed (FS) sagittal proton density-weighted images (PDWI), non-FS coronal PDWI, FS coronal PDWI, non-FS axial PDWI, and FS axial PDWI, were also included in the protocol. This was done to confirm the normal appearance of each knee, as well as for use in future clinical applications.

### Image processing and cartilage segmentation of entire knee

Images were transferred in DICOM (Digital Imaging and Communications in Medicine) format to a personal computer (PC; Windows 7), which was used to perform all post-processing and analyses. For possible motion between scans, T1rho series were first realigned relative to the first TSL images using rigid-body transformation before being fitted to mono-exponential function on a pixel-by-pixel basis for generation of T1rho maps:  $S(TSL) = S_0 \times \exp(-TSL/T1rho)$ , where  $S_0$  is the signal intensity when  $TSL=0$ . The cartilage of the entire femur was extracted slice-by-slice by T.N., a board-certified radiologist of the Japanese College of Radiology, with 13 years of experience and subspecialization in musculoskeletal radiology.  $TSL=20$  was

**Table 1** Methodology of cartilage segmentation in T1rho analyses from prior studies

Reference	No. slices	Compartment	Angle measurement	Depth analysis
Schooler et al. [14]	Multiple slices	2 (MFC/MT)	None	bone/articular
Gupta et al. [31]	Slice by slice	49 (LFC, MFC, LT, MT, patella)	Anterior/central/posterior	Superficial/deep
Theologis et al. [28]	No detail	LFC/MFC, LT/MT, patella	LFC/MFC - 5 sublesions, Tibia - 3 sublesions	None
Peers et al. [23]	No detail	3 (medial, central, lateral)	WB/NWB	None
Wang et al. [13]	No detail	12 (LFC/MFC, LT/MT)	Anterior/central/posterior	None
Hirose et al. [16]	1 slice	LFC/MFC, LT/MT	WB/NWB	None
Wong et al. [18]	Whole slice	LT	None	None
Takayama et al. [19]	No detail	Orthopaedic surgeon's instruction	None	None
Souza et al. [21]	No detail	4 (LFC/MFC, LT/MT)	None	None
Su et al. [27]	No detail	LFC/MFC, LT/MT	5 sublesions	Superficial/deep
Goto et al. [15]	No detail	LFC/MFC, LT/MT	WB/NWB	None
Wang et al. [20]	No detail	16 (LFC/MFC, LT/MT)	Anterior/central/posterior	None
Tsushima et al. [22]	No detail	None	None	Superficial/deep
Theologis et al. [29]	No detail	N/A	N/A.	Superficial/deep
Li et al. [26]	No detail	LFC/MFC, LT/MT	5 sublesions	Superficial/deep
Li et al. [25]	No detail	LT/MT, LFC/MFC	Anterior/posterior and 0°, 54.7°, 90°	None
Zhao et al. [30]	No detail	LFC/MFC, LT/MT, patella	N/A	None
Zarins et al. [32]	No detail	LFC/MFC, LT/MT, patella	None	None
Stahl et al. [17]	No detail	LFC/MFC, LT/MT, trochlea, patella	MFC/LFC-WB/NWB	None
Bolbos et al. [24]	No detail	LFC/MFC, LT/MT	MFC/LFC-WB, NWB (anterior, posterior)	None

MFC medial femoral condyle, MT medial tibia, LFC lateral femoral condyle, LT lateral tibia, WB weight-bearing, NWB non-weight-bearing

specifically chosen for segmentation because the shortest spin-lock length has the highest signal-to-noise ratio. The shortest TSL was used for segmentation of cartilage in a prior study [20]. Once cartilage was segmented by manually placing vertices along the boundary, their  $x$  and  $y$  coordinates were used in a circle-fitting algorithm by assuming a circular cartilage shape around an imaginary centre position in the subchondral bone, whose coordinates were estimated in a least squares manner, and which the user could manually place instead if necessary. Additional boundary vertices with finer spacing were then interpolated and used for computation of slope angles for the radial vectors from the centre position to each boundary vertex. For each slope angle (in 1° increments) the farthest (closest to the articular surface) and nearest (closest to the bone) boundary vertices were recorded, while the radial points between the boundary vertices were approximated by linear interpolation and recorded for subsequent depth/angle-based segmentation of cartilage. The T1rho depth/angle-dependent profile was investigated in this study by partitioning cartilage into two layers (deep, 51–100 %; superficial, 0–50 %) and angular segmentation in increments of 4° over the length of segmented cartilage (the angle 0 defined along B0) with positive/negative angles in a counterclockwise/clockwise rotation (Fig. 1). The method of partitioning of the cartilage into two halves was described in several recent studies [33, 34]. All image processing described

above was performed using in-house-developed and implemented software in MATLAB (The MathWorks, Inc., Natick, MA, USA). Bland–Altman plot-based investigation of the inter- and intra-operator agreement in manual cartilage segmentation of the same data set was carried out and published previously [35]. The measured mean difference in the size of individual angular segments and limits of agreement (95 %, expressed as  $\pm 2$  SD) in number of pixels were  $-1.4 \pm 15.5$  and  $2.5 \pm 19.4$ , respectively, for the inter- and intra-operator agreement, while those converted into area ( $\text{mm}^2$ ) were  $-0.11 \pm 1.16$  and  $0.19 \pm 1.45$ , respectively.

### Normalization of entire femoral cartilage

After slice-by-slice manual segmentation of the entire femoral cartilage, it was normalized for all subjects with different knee sizes. This was performed utilizing the same method described in a prior study [36]. First, we reformatted coronal sections from sagittal images of knee 3D MRI data using the Medical Image Processing, Analysis and Visualization (MIPAV; Center for Information Technology, National Institutes of Health, Bethesda, MD, USA) software, and determined the centre of the medial femoral condyle (MC), lateral femoral condyle (LC), and femoral trochlea (T). From each of these three anatomical landmarks (MC, LC, T) new

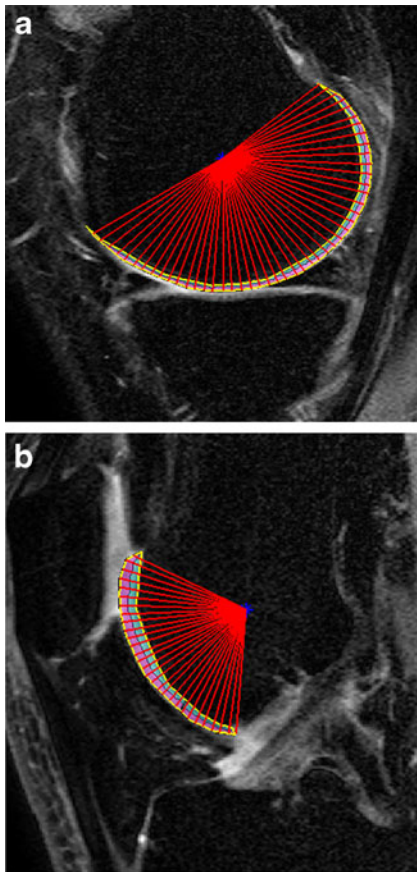


**Fig. 1** Sagittal SPGR images in the section of the (a) medial condyle and the (b) trochlea from T1rho sequences after manual segmentation with post-processing. After manual segmentation, angular analysis with in step of 4°, and depth analysis of the superficial and deep layers was performed

slices of 3-mm thickness were defined (e.g., MC+3, MC+6, T-3) for all subjects. By matching these new slices and calculating their average T1rho values for each subject, we normalized the entire femoral cartilage into 23 new slices, which were calculated and obtained from the average transverse diameter (68.9 mm) of the femoral cartilage of the 20 healthy volunteers.

### 3D T1rho map of normalized femoral cartilage and analysis of T1 rho values

We calculated the average T1rho values of cartilage over each anatomical landmark and the entire femur on each normalized knee in both the superficial and deep layer with 4° stepwise analysis. In addition, we compared the average T1rho values at representative angles of -54°, -30°, 0°, +30°, and +54° to evaluate angle dependent change, including the magic angle effect, as described in a prior paper [36]. The weight-bearing effect was evaluated by dividing the articular cartilage into weight-bearing and non-weight-bearing portions, with definition of the angle from -30° to +30° as weight-bearing, and

angles smaller than -30° or greater than 30° as non-weight-bearing [37]. Finally, we created 3D graphs and surface maps of the T1rho profiles using R version 3.0.2 for Windows software (R Development Core Team, Vienna, Austria) and MATLAB. In creating 3D graphs, we used the thin-plate spline method as an interpolant [38].

### Statistical analysis

The differences in T1rho values between superficial and deep layers, and between weight-bearing and non-weight-bearing areas, were statistically analysed using the Wilcoxon signed-rank test. A  $p$  value <0.05 was considered to be statistically significant.

Statistical analyses were performed using R version 3.0.2 for Windows software (R Development Core Team, Vienna, Austria).

## Results

### Angle-and depth dependence of T1rho profiles

Figure 2 shows the T1rho profiles of each layer with angle-dependent analysis at the medial condyle, lateral condyle, and trochlea. In the medial and lateral condyles, T1rho values were higher in the superficial layer than in the deep layer in most locations, including the weight-bearing portion. In the trochlea, T1rho values were higher in the superficial layer than the deep layer above approximately -50°, and an inverse relationship appeared below -50°, with higher T1rho values in the deep layer. Throughout each anatomical landmark (MC, LC, T), T1rho values were not constant, even within the weight-bearing portion (-30 to +30°) of the medial and lateral condyles. Angular variations among the T1rho profiles in each layer demonstrated no influence of magic angle effect. Figure 3 shows the average cartilage T1rho values in each layer at the anatomical landmarks and the entire femur. Average T1rho values in the superficial layer of the femoral articular cartilage were higher than those in the deep layer over the entire femur, medial condyle, and lateral condyle, with significant difference ( $p < 0.05$ ). The difference in T1rho values between the two layers at the trochlea, however, were not statistically significant.

Table 2 shows the average cartilage T1rho values of the weight-bearing and non-weight-bearing portions of the entire femur, medial femoral condyle, and lateral femoral condyle. T1rho values of the deep layer of the weight-bearing portions of the medial and lateral condyles were lower than those of the non-weight-bearing portions, with a statistically significant difference ( $p < 0.05$ ). In contrast, there was no significant difference in T1rho values of the



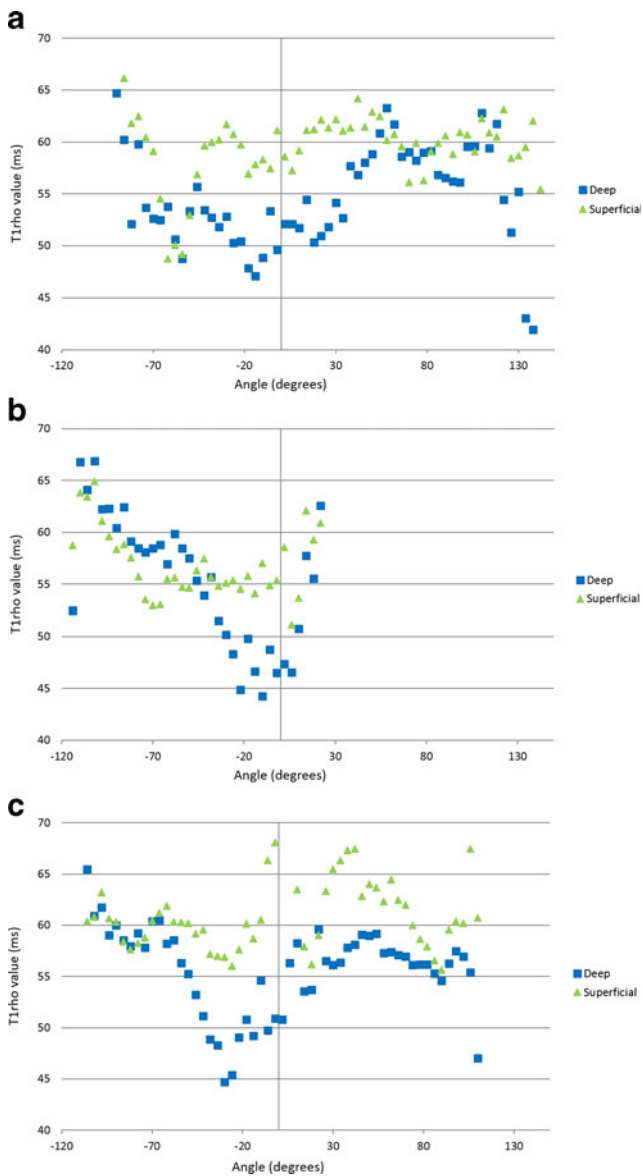


**Fig. 2** Angle-dependent analysis of T1rho values of the superficial and deep layers at the (a) medial condyle, (b) trochlea, and (c) lateral condyle. There is angle dependence of T1rho profiles in each layer, with no influence of magic angle effect. T1rho values are higher in the superficial layer than the deep layer in most areas of the medial and lateral condyles. At the trochlea, T1rho values are higher in the superficial layer compared to the deep layer at above approximately  $-50^\circ$ , and an inverse relationship appears below  $-50^\circ$ , with higher T1rho values in the deep layer. Average T1rho values in the superficial layer of the femoral articular cartilage are higher than those in the deep layer on the (a) medial condyle, and (c) lateral condyle, with a statistically significant difference ( $p < 0.05$ )

superficial layer between the weight-bearing and non-weight-bearing portions.

Table 3 shows the average T1rho values at representative angles. There was no influence of a magic angle effect on T1rho values, although there was angular variation in each layer. Again, T1rho values in the deep layer were lower than those in the superficial layer at all representative angles.

### 3D graphs and surface maps of T1rho profile

Figure 4 demonstrates 3D graphs of T1rho mapping. Figure 4a is a 3D coloured map of T1rho from the whole layer of the entire femoral condyle illustrating the differences among T1rho values. The remaining graphs reveal three-dimensional T1rho values in the superficial, deep, and whole layers of the entire femoral condyle, viewed by different sections (Fig. 4b-d). Each layer is represented by a single colour tone. It is well demonstrated here that cartilage T1rho values were not homogeneous throughout the entire femoral condyle.

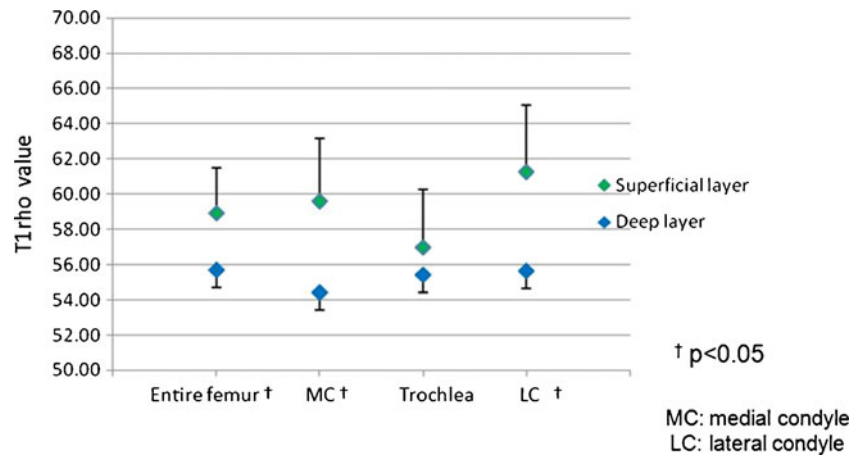
Figure 5 shows projection maps of mean T1rho profiles of normalized femoral cartilage, with 23 slices in each layer. The colour bar indicates *red* for high, *green* for middle, and *blue* for low T1rho values. T1rho values tended to be lower within the deep layer of the weight-bearing portion, and were not homogeneous in each layer throughout the entire femoral condyle. There was a focal area of decreased T1rho values in the deep layers of the inferior trochlea and the anterior aspect of the lateral femoral condyle, as seen in Fig. 2b and c.

### Discussion

In this study, we presented several new findings regarding the T1rho profile for the entire femoral cartilage, utilizing a depth/angle-dependent analysis. First, our results demonstrated angle- and depth-dependent variations in the T1rho profile for each layer, with no influence of a magic angle effect. Second, we created normalized T1rho profiles of healthy femoral cartilage based on three-dimensional angle-and depth-dependent analysis utilizing surface maps and 3D graphs. This analysis demonstrated that T1rho values were not homogeneous in each layer throughout the entire femoral condyle.

With respect to comparisons between weight-bearing and non-weight-bearing portions, Goto et al. reported that T1rho values in normal asymptomatic volunteers were higher in weight-bearing regions of the medial femoral cartilage than in less-weight-bearing regions. On the other hand, in the lateral femoral condyle, they found no significant difference in T1rho values between weight-bearing and less-weight-bearing regions [15]. In contrast, in a study of ACL injury patients and controls, Bolbos et al. found significantly higher T1rho values within the non-weight-bearing versus weight-bearing portions of the femoral condyle [24]. Thus these two studies demonstrated opposite results. In our study, T1rho values were higher in the non-weight-bearing portion than in the weight-bearing portion over the medial and lateral condyles, which supports the results of the Bolbos et al. study. This finding is more significant in the deep layer. In other words, proteoglycan content was greater and T1rho values were lower in the weight-bearing portion, especially in the deep layer. In the analysis of depth and angle dependence, it

**Fig. 3** Difference in average T1rho values between the superficial and deep layers at the medial condyle, lateral condyle, trochlea, and the entire femoral cartilage. Average T1rho values in the superficial layer of the femoral articular cartilage are higher than in the deep layer over the entire femur, medial condyle, and lateral condyle, with a statistically significant difference ( $p < 0.05$ )



is important to note that cartilage has an organized and layered structure, divided into four zones: the superficial zone, middle zone, deep zone, and zone of calcified cartilage. Chondrocytes in the superficial zone secrete relatively little proteoglycan [39, 40]. In contrast, the deep zone contains the highest proteoglycan concentration. Proteoglycans resist compression, and generate swelling pressure due to their affinity for water. The deep zone consists of large-diameter collagen fibrils oriented perpendicular to the articular surface. This layer contains the highest proteoglycan and lowest water concentrations, and has the highest compressive modulus [41]. More resistance to various forces in knee activity is required in the weight-bearing portion. Therefore, it makes sense that cartilage in the weight-bearing portion needs more proteoglycan, which results in lower T1rho values in this region, as seen in the present study. Furthermore, we postulate that the

difference in T1rho values between the two previously mentioned studies may be due to the methodology of segmentation and ROI placement. ROIs were manually drawn by Goto et al. in a portion of the cartilage within the medial and lateral condyles, and they did not utilize entire slices for femoral cartilage segmentation [15]. Our study demonstrates that T1rho values are not constant throughout the femoral condyle and trochlea, even within the weight-bearing portions (−30 to +30°) of the medial and lateral condyles. For example, there is a minimal peak of T1rho values in the deep layer at approximately −10 to −20° within the trochlea and −30° within the lateral condyle (Figs. 2b, c and 5c). These locations correspond to cartilage of the distal trochlea and anterior to the lateral femoral notch. Yoshioka et al. reported that 3D SPGR images showed non-uniform signal intensity within articular cartilage of the knee, and signal intensity was decreased in these locations [42].

**Table 2** Average T1rho values of weight-bearing and non-weight-bearing portions of the entire femoral cartilage, medial femoral condyle, and lateral femoral condyle

		Angle	Depth	T1rho value (mean±SD)
Entire femur		(−180~180)	Whole	56.97±2.82
			Superficial	58.94±2.56
			Deep	55.68±3.55
MC	Non-weight-bearing	(< − 30,30<)	Whole	57.50±4.06*
			Superficial	59.51±4.07
			Deep	55.67±5.42**
	Weight-bearing	(−30~30)	Whole	54.91±1.33*
			Superficial	59.81±1.85
			Deep	51.13±2.11**
LC	Non-weight-bearing	(< − 30,30<)	Whole	58.64±2.47***
			Superficial	60.92±2.95
			Deep	56.96±3.56****
	Wieght-bearing	(−30~30)	Whole	55.51±3.34***
			Superficial	62.11±5.35
			Deep	52.46±4.36****

Paired symbols (\*, \*\*, \*\*\*, \*\*\*\*) denote comparisons where a statistically significant difference (all,  $p < 0.05$ ) in T1rho values is detected.

MC medial condyle, LC lateral condyle

**Table 3** Average T1rho values at representative angles

	Angle	Depth	T1 rho value (mean±SD)
Entire femur	−54	Whole	54.58±6.23
		Superficial	55.02±6.94**
		Deep	54.48±5.37****
	−30	Whole	53.58±2.84*
		Superficial	56.84±4.22***
		Deep	50.79±3.39*****
	0	Whole	55.92±3.74* † ††
		Superficial	61.01±5.47***
		Deep	53.47±4.65***** †††
	30	Whole	58.12±3.13†
		Superficial	61.48±3.98
		Deep	55.56±3.33††††
54	Whole	59.24±2.83††	
	Superficial	60.81±3.70	
	Deep	58.37±2.69 ††† ††††	

Paired symbols (\*, \*\*, †, etc.) denote comparisons where a statistically significant difference (all,  $p < 0.05$ ) in T1rho values is detected. Asterisk (\*) is used for statistically significant difference between values from  $-54^\circ$  to  $0^\circ$ . Dagger (†) is used for statistically significant difference between values from  $0^\circ$  to  $54^\circ$ .

Hypointense regions of the articular cartilage are known to correspond to collagenous tissue or extracellular matrix [43, 44], with an associated decrease in T1rho values as collagen content increases [45]. There is also evidence that several factors other than proteoglycan depletion may contribute to variations in T1rho values. These include collagen fibre orientation/concentration and the concentration of other macromolecules [6, 46]. The distal trochlea is likely non-weight-bearing. Therefore, the minimal peak of cartilage T1rho in the distal trochlea seems to be mainly attributable to an increase in collagen content.

In our study, cartilage T1rho values over the trochlea showed less difference between the superficial and deep layers. Those values above and below approximately  $-50^\circ$  demonstrated an inverse relationship. One reason for this is that the trochlea appears to be less weight-bearing, and thus less proteoglycan is necessary in the deep layer. The other reason is that T1rho values in the superficial layer of the trochlea were decreased below  $-50^\circ$  in the area where the trochlea opposes the patella. During flexion and extension of the knee, the patella moves back and forth inside the trochlear groove. The increase in shear stress within the superficial layer of the trochlea may require more collagen, since type II collagen contributes to the shear and tensile properties of the tissue [41]. This finding may explain the decrease in T1rho of the superficial layer over the trochlea at the patellofemoral joint.

Researchers have also reported observing a magic angle effect for T1rho relaxation time in the study of human

osteoarthritic cartilage specimens [25]. However, our results showed no significant magic angle effect on T1rho profiles, although there were angle-dependent variations in both superficial and deep layers and a subtle nonspecific peak in the deep layer of the medial femoral condyle between  $+50^\circ$  and  $+70^\circ$ . Additionally, 3D graphs and 2D surface maps failed to demonstrate an apparent peak at  $54^\circ$ .

We were able to compare T1rho values from throughout the entire femoral cartilage with previously reported results at specific locations [15, 17, 21, 24, 26]. Two different 3D graphs based on thin-plate spline, and two dimensional (2D) projection maps of T1rho values in normalized femoral cartilage with a colour-bar help us to visualize and understand T1rho variations within the entire femoral condylar cartilage. With a 3D graph, we are able to recognize the differences in T1rho values more stereographically. In laminar analysis, the 3D graph with all layers is more comprehensible (Fig. 4b–d). However, the 3D graph has the disadvantage of overestimating or underestimating T1rho values because of the effect of interpolation [47]. A 2D surface map in this study showed two-dimensional projection of T1rho values, which will enable easier comparison of normalized volunteer data with patient data in clinical applications. We were able to analyse T1rho values three-dimensionally across the entire femoral condyle utilizing 3D graphs and surface maps from various points of view, including angle, layer, slice, and anatomic landmark. These improve upon previously reported 2D analyses with several slices from the knee. We believe that 3D graph and surface map analysis of the entire femoral condyle is one of the most promising tools for cartilage T1rho analysis. This method can also be easily applied to T2 map analysis.

From a clinical perspective, it is important to understand that T1rho values have angle/depth-dependent variations among the various anatomical landmarks. In this study, these appeared to be influenced by water, collagen, and proteoglycan content in various locations and to various degrees, with little influence of collagen orientation. Therefore, detailed T1rho profiles of the standardized entire normal femoral cartilage could serve as a baseline for investigating pathological conditions of knee cartilage. These findings may be particularly helpful for the accurate diagnosis of early cartilage degeneration, i.e. early OA, and within a specific location and depth within the cartilage.

Our study has several limitations. First, the study sample was small. According to a power analysis based on a two-sample  $t$  test model of equal allocation and variance, and using previously published data [32], the sample size ( $n=20$ ) yielded 75 % power at a significance level of 0.05 ( $\alpha=0.05$ ). In the future, we will need T1rho data from normalized entire knee cartilage for much larger samples in order to improve accuracy. Second, the superficial and deep layers we analysed do not correlate with the four physiologic zones of



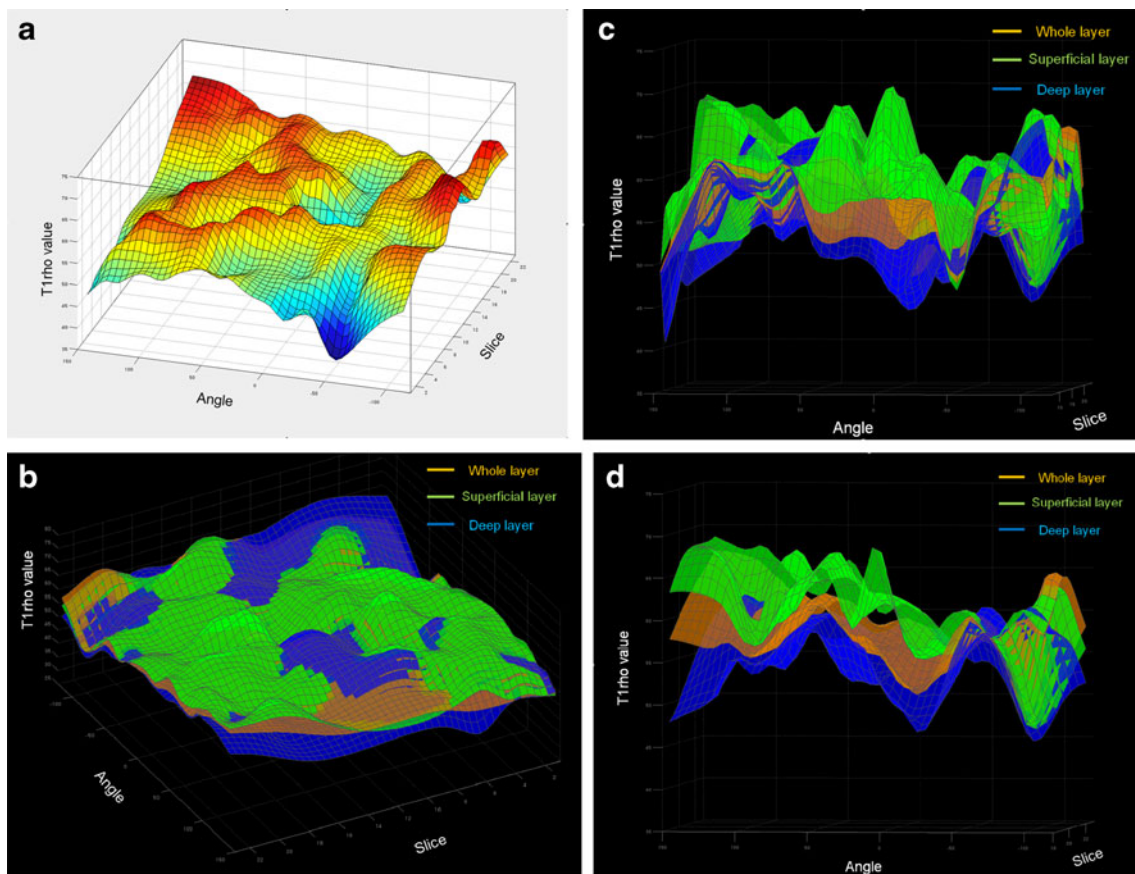


**Fig. 4** 3D graphs of T1rho mapping of normalized femoral cartilage based on thin-plate spline, demonstrating that T1rho values are not homogeneous over the entire femoral cartilage. (a) single-layer 3D graph was coloured on the basis of the difference of T1rho values. (b)

A 3D graph with a single colour tone per layer, with simultaneous expression of the superficial, deep, and whole layers. (c) Cross-section image of the medial condyle from figure 4B. (d) Cross-section image of the lateral condyle from figure 4B

articular cartilage [41]. It is an inevitable technical limitation that the spatial resolution is not sufficient to distinguish four physiologic layers. Third, there is limitation in normalizing the entire femoral cartilage. A measurement error will become larger as the distance from the each landmark becomes greater, because the size of femoral cartilage is different among subjects. To fix this problem, we need to analyse larger samples, which will reduce the measurement error in normalization for future studies. Fourth, we must consider rotation effects in the longitudinal/transverse axis of subjects. Because each knee of the subject is placed in a slightly flexed and rotated position in the coil, obtained sagittal images were not completely matched in longitudinal/transverse axis. However, since sagittal images were obtained without oblique angulation, parallel to the B0, we believe we have minimized the difference of rotation effects, especially for the magic angle effect. Fifth, it was outside the scope of our study to assess the effect of varus/valgus malalignment and deviation of the leg axis. Varus and valgus knee malalignment influences the distribution of load at the knee joint and has been shown to be a possible factor for OA [48]. Finally, it was time-consuming to extract the entire femoral cartilage data by manual segmentation and analyse

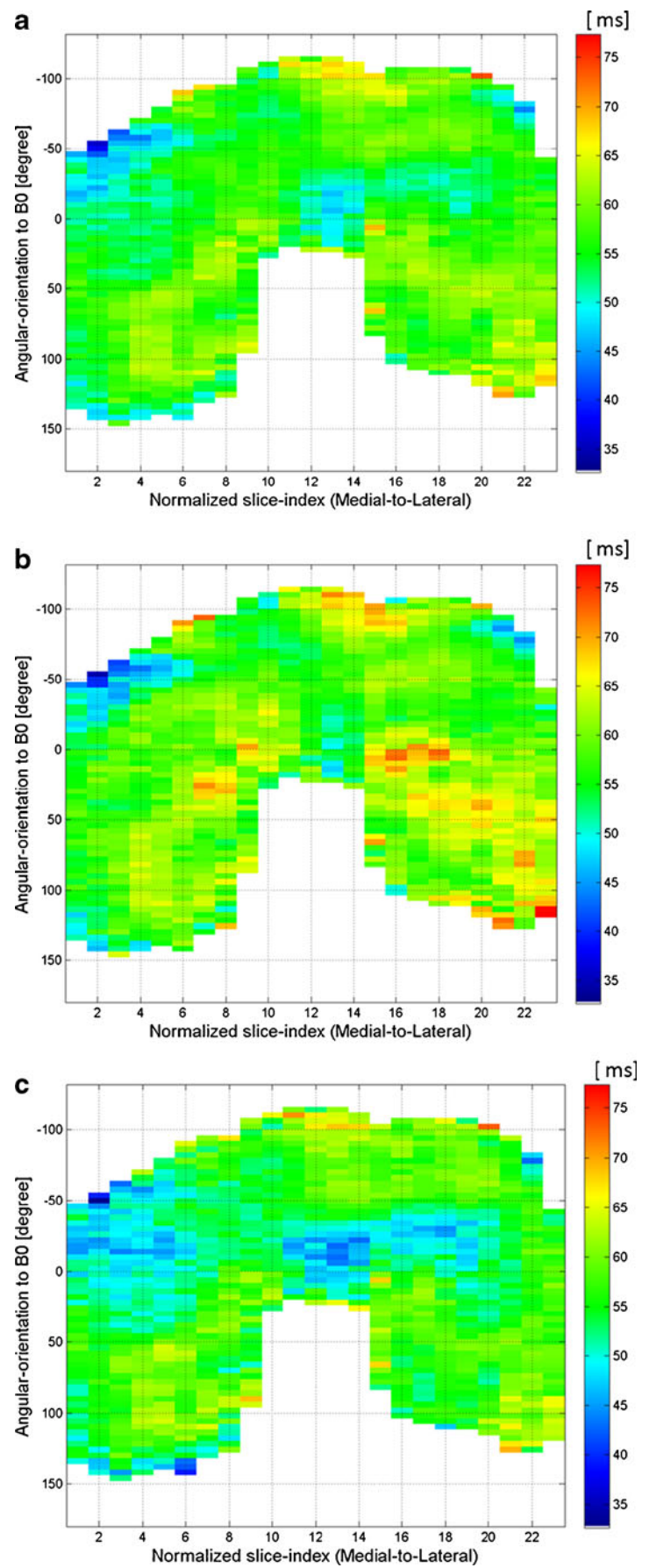
T1rho values with 3D graphs and surface maps. Therefore, it is clinically and practically difficult to process knee samples from a large number of patients using our manual method. Further technical development of auto-segmentation and auto-3D analysis is needed in order to efficiently apply this form of analysis to patient data in clinical practice.

In conclusion, T1rho values of the femoral cartilage demonstrate regional and depth variation, with lower T1rho values in the deep layer and no significant magic angle effect. T1rho values across the entire femoral condyle can be analysed three-dimensionally by utilizing 3D graphs and surface maps using different display parameters. It is important to understand the normal T1rho variations that occur throughout the entire knee cartilage in order to detect early T1rho abnormalities and early OA in clinical applications.

**Acknowledgments** The authors thank Dr. Andrew Chang, M.D., for preparation of the manuscript.

The scientific guarantor of this publication is Hiroshi Yoshioka. The authors of this manuscript declare no relationships with any companies whose products or services may be related to the subject matter of the article. This study has received funding by the National Center for Research Resources and the National Center for Advancing Translational

**Fig. 5** 2D surface maps of the T1rho profile of normalized femoral cartilage with 23 slices. The *colour bar* indicates *red* for high, *green* for middle, and *blue* for low T1rho values. **(a)** Whole layer. **(b)** Superficial layer. **(c)** Deep layer



Sciences, National Institutes of Health, through Grant UL1 TR000153. One of the authors has significant statistical expertise.

Institutional review board approval was obtained. Written informed consent was obtained from all subjects (patients) in this study. Methodology: prospective, experimental, performed at one institution.

**Open Access** This article is distributed under the terms of the Creative Commons Attribution-NonCommercial 4.0 International License (<http://creativecommons.org/licenses/by-nc/4.0/>), which permits any non-commercial use, distribution, and reproduction in any medium, provided you give appropriate credit to the original author(s) and the source, provide a link to the Creative Commons license, and indicate if changes were made.

## Reference

- Lawrence RC, Felson DT, Helmick CG et al (2008) Estimates of the prevalence of arthritis and other rheumatic conditions in the United States. Part II. *Arthritis Rheum* 58:26–35
- Puig-Junoy J, Ruiz Zamora A (2015) Socio-economic costs of osteoarthritis: A systematic review of cost-of-illness studies. *Semin Arthritis Rheum* 44:531–41
- Smelter E, Hochberg MC (2013) New treatments for osteoarthritis. *Curr Opin Rheumatol* 25:310–316
- Choi JA, Gold GE (2011) MR imaging of articular cartilage physiology. *Magn Reson Imaging Clin N Am* 19:249–282
- Gold GE, Burstein D, Dardzinski B, Lang P, Boada F, Mosher T (2006) MRI of articular cartilage in OA: novel pulse sequences and compositional/functional markers. *Osteoarthritis Cart* 14(Suppl A): A76–86
- Crema MD, Roemer FW, Marra MD et al (2011) Articular cartilage in the knee: current MR imaging techniques and applications in clinical practice and research. *Radiographics* 31:37–61
- Bittersohl B, Miese FR, Dekkers C et al (2013) T2\* mapping and delayed gadolinium-enhanced magnetic resonance imaging in cartilage (dGEMRIC) of glenohumeral cartilage in asymptomatic volunteers at 3 T. *Eur Radiol* 23:1367–74
- Raya JG, Dettmann E, Notohamiprodjo M, Krasnokutsky S, Abramson S, Glaser C (2014) Feasibility of in vivo diffusion tensor imaging of articular cartilage with coverage of all cartilage regions. *Eur Radiol* 24:1700–6
- Goodwin DW, Wadghiri YZ, Dunn JF (1998) Micro-imaging of articular cartilage: T2, proton density, and the magic angle effect. *Acad Radiol* 5:790–798
- Akella SV, Regatte RR, Gougoutas AJ et al (2001) Proteoglycan-induced changes in T1rho-relaxation of articular cartilage at 4T. *Magn Reson Med* 46:419–423
- Borthakur A, Mellon E, Niyogi S, Witschey W, Kneeland JB, Reddy R (2006) Sodium and T1rho MRI for molecular and diagnostic imaging of articular cartilage. *NMR Biomed* 19:781–821
- Watanabe A, Boesch C, Siebenrock K, Obata T, Anderson SE (2007) T2 mapping of hip articular cartilage in healthy volunteers at 3T: a study of topographic variation. *J Magn Reson Imaging* 26: 165–171
- Wang L, Vieira RL, Rybak LD et al (2013) Relationship between knee alignment and T1rho values of articular cartilage and menisci in patients with knee osteoarthritis. *Eur J Radiol* 82:1946–1952
- Schooler J, Kumar D, Nardo L et al (2014) Longitudinal evaluation of T1rho and T2 spatial distribution in osteoarthritic and healthy medial knee cartilage. *Osteoarthritis Cart* 22:51–62
- Goto H, Iwama Y, Fujii M et al (2012) A preliminary study of the T1rho values of normal knee cartilage using 3T-MRI. *Eur J Radiol* 81:e796–803
- Hirose J, Nishioka H, Okamoto N et al (2013) Articular cartilage lesions increase early cartilage degeneration in knees treated by anterior cruciate ligament reconstruction: T1rho mapping evaluation and 1-year follow-up. *Am J Sports Med* 41:2353–2361
- Stahl R, Luke A, Li X et al (2009) T1rho, T2 and focal knee cartilage abnormalities in physically active and sedentary healthy subjects versus early OA patients—a 3.0-Tesla MRI study. *Eur Radiol* 19:132–143
- Wong CS, Yan CH, Gong NJ, Li T, Chan Q, Chu YC (2013) Imaging biomarker with T1rho and T2 mappings in osteoarthritis—in vivo human articular cartilage study. *Eur J Radiol* 82:647–650
- Takayama Y, Hatakenaka M, Tsushima H et al (2013) T1rho is superior to T2 mapping for the evaluation of articular cartilage denaturalization with osteoarthritis: radiological–pathological correlation after total knee arthroplasty. *Eur J Radiol* 82:e192–198
- Wang L, Chang G, Xu J et al (2012) T1rho MRI of menisci and cartilage in patients with osteoarthritis at 3T. *Eur J Radiol* 81:2329–2336
- Souza RB, Feeley BT, Zarins ZA, Link TM, Li X, Majumdar S (2013) T1rho MRI relaxation in knee OA subjects with varying sizes of cartilage lesions. *Knee* 20:113–119
- Tsushima H, Okazaki K, Takayama Y et al (2012) Evaluation of cartilage degradation in arthritis using T1rho magnetic resonance imaging mapping. *Rheumatol Int* 32:2867–2875
- Peers SC, Maerz T, Baker EA et al (2014) T1rho magnetic resonance imaging for detection of early cartilage changes in knees of asymptomatic collegiate female impact and nonimpact athletes. *Clin J Sport Med* 24:218–225
- Bolbos RI, Ma CB, Link TM, Majumdar S, Li X (2008) In vivo T1rho quantitative assessment of knee cartilage after anterior cruciate ligament injury using 3 Tesla magnetic resonance imaging. *Invest Radiol* 43:782–788
- Li X, Cheng J, Lin K et al (2011) Quantitative MRI using T1rho and T2 in human osteoarthritic cartilage specimens: correlation with biochemical measurements and histology. *Magn Reson Imaging* 29:324–334
- Li X, Kuo D, Theologis A et al (2011) Cartilage in anterior cruciate ligament-reconstructed knees: MR imaging T1{rho} and T2—initial experience with 1-year follow-up. *Radiology* 258:505–514
- Su F, Hilton JF, Nardo L et al (2013) Cartilage morphology and T1rho and T2 quantification in ACL-reconstructed knees: a 2-year follow-up. *Osteoarthritis Cart* 21:1058–1067
- Theologis AA, Haughom B, Liang F et al (2014) Comparison of T1rho relaxation times between ACL-reconstructed knees and contralateral uninjured knees. *Knee Surg Sports Traumatol Arthrosc* 22:298–307
- Theologis AA, Schairer WW, Carballido-Gamio J, Majumdar S, Li X, Ma CB (2012) Longitudinal analysis of T1rho and T2 quantitative MRI of knee cartilage laminar organization following microfracture surgery. *Knee* 19:652–657
- Zhao J, Li X, Bolbos RI, Link TM, Majumdar S (2010) Longitudinal assessment of bone marrow edema-like lesions and cartilage degeneration in osteoarthritis using 3 T MR T1rho quantification. *Skeletal Radiol* 39:523–531
- Gupta R, Virayavanich W, Kuo D et al (2014) MR Trho quantification of cartilage focal lesions in acutely injured knees: correlation with arthroscopic evaluation. *Magn Reson Imaging* 32:1290–6
- Zarins ZA, Bolbos RI, Pialat JB et al (2010) Cartilage and meniscus assessment using T1rho and T2 measurements in healthy subjects and patients with osteoarthritis. *Osteoarthritis Cart* 18:1408–1416
- Carballido-Gamio J, Stahl R, Blumenkrantz G, Romero A, Majumdar S, Link TM (2009) Spatial analysis of magnetic resonance T1rho and T2 relaxation times improves classification

- between subjects with and without osteoarthritis. *Med Phys* 36: 4059–4067
34. Multanen J, Rauvala E, Lammentausta E et al (2009) Reproducibility of imaging human knee cartilage by delayed gadolinium-enhanced MRI of cartilage (dGEMRIC) at 1.5 Tesla. *Osteoarthritis Cart* 17:559–564
  35. Nozaki T, Kaneko Y, Yu HJ, Kaneshiro K, Schwarzkopf R, Yoshioka H (2015) Comparison of T1rho imaging between spoiled gradient echo (SPGR) and balanced steady state free precession (b-FFE) sequence of knee cartilage at 3T MRI. *Eur J Radiol* 84:1299–1305
  36. Kaneko Y, Nozaki T, Yu H et al. (2015) Normal T2 map profile of the entire femoral cartilage using an angle/layer-dependent approach. *J Magn Reson Imaging* (Published in Early View)
  37. Stahl R, Blumenkrantz G, Carballido-Gamio J et al (2007) MRI-derived T2 relaxation times and cartilage morphometry of the tibio-femoral joint in subjects with and without osteoarthritis during a 1-year follow-up. *Osteoarthritis Cart* 15:1225–1234
  38. Bookstein FL (1989) Principal warps: Thin-plate splines and the decomposition of deformations. *IEEE Trans Pattern Anal Mach Intell* 11:567–585
  39. Larsson SE, Lemperg RK (1974) The glycosaminoglycans of the different layers of bovine articular cartilage in relation to age. II. Incorporation of <sup>35</sup>S-sulphate in vitro into different fractions of chondroitin sulphate. *Calcif Tissue Res* 15:253–267
  40. Venn M, Maroudas A (1977) Chemical composition and swelling of normal and osteoarthrotic femoral head cartilage. I. Chemical composition. *Ann Rheum Dis* 36:121–129
  41. Pearle AD, Warren RF, Rodeo SA (2005) Basic science of articular cartilage and osteoarthritis. *Clin Sports Med* 24:1–12
  42. Yoshioka H, Stevens K, Genovese M, Dillingham MF, Lang P (2004) Articular cartilage of knee: normal patterns at MR imaging that mimic disease in healthy subjects and patients with osteoarthritis. *Radiology* 231:31–38
  43. Goodwin DW, Zhu H, Dunn JF (2000) In vitro MR imaging of hyaline cartilage: correlation with scanning electron microscopy. *AJR Am J Roentgenol* 174:405–409
  44. Waldschmidt JG, Rilling RJ, Kajdacsy-Balla AA, Boynton MD, Erickson SJ (1997) In vitro and in vivo MR imaging of hyaline cartilage: zonal anatomy, imaging pitfalls, and pathologic conditions. *Radiographics* 17:1387–1402
  45. Menezes NM, Gray ML, Hartke JR, Burstein D (2004) T2 and T1rho MRI in articular cartilage systems. *Magn Reson Med* 51: 503–509
  46. Mlynarik V, Trattnig S, Huber M, Zembsch A, Imhof H (1999) The role of relaxation times in monitoring proteoglycan depletion in articular cartilage. *J Magn Reson Imaging* 10:497–502
  47. Sharma G, Shaw MQ (2006) Thin-plate splines for printer data interpolation. *Proceedings of European Signal Processing Conference (EUSIPCO)*, Florence, Italy, September 4–8
  48. Sharma L, Song J, Felson DT, Cahue S, Shamiyeh E, Dunlop DD (2001) The role of knee alignment in disease progression and functional decline in knee osteoarthritis. *JAMA* 286:188–195